# Asymmetrical Bidirectional DC–DC Converter With Limited Reverse Power Rating in Smart Transformer

Rongwu Zhu, *Member, IEEE*, Felix Hoffmann, *Student Member, IEEE*, Nimrod Vázquez, *Senior Member, IEEE*, Kangan Wang, and Marco Liserre, *Fellow, IEEE*

***Abstract*—The increasing penetration of distributed generators in low-voltage distribution grids may lead to distribution transformers, also a smart transformer, experiencing the reverse power flow, which is less as compared to the forward power flow in the current electric grid. This article proposes an asymmetrical bidirectional dc–dc (AB-DC/DC) converter, which has two partial-scale rectifiers of an active bridge and a diode bridge connected in parallel at the secondary side, with less cost of power semiconductors and the capability of bidirectional operation to satisfy the realistic condition. The proposed AB-DC/DC converter works as a single active bridge under forward power flow condition, while it works as a dual active bridge under reverse power flow condition. The solutions to share the active power under forward operation and suppress the circulating power under reverse operation are proposed, respectively. The simulation and experimental results both clearly validate the effectiveness and feasibility of the proposed AB-DC/DC converter.**

***Index Terms*—Asymmetrical bidirectional dc–dc (AB-DC/DC) converter, dual active bridge (DAB), smart transformer (ST).**

## I. Introduction

A SMART transformer (ST) can provide the dc connectivity and reduce grid reinforcements caused by integration of high penetration of distributed generator (DG) and electric vehicle (EV) charging stations [1]–[3]. Thus, the ST is a promising solution for increasing the hosting capability of DG and EV charging stations in low-voltage (LV) distribution grids [1].

Generally, the direction of power flow in distribution transformers, also the ST, is from the medium-voltage (MV) to the LV side. This feature only requires the unidirectional operation capability of an ST (forward operation mode). However, due to the continuously increasing penetration of DGs and the asynchronous behavior between the power generation of DGs and the power consumption in loads, the ST will experience reverse power flow (i.e., from LV to MV side) [4]–[6]. Compared to the forward power flow, which can reach the rated power of the ST, the reverse power is less and only appears few hours per day [4]. Such behavior indicates that if the power-electronics-based ST is designed with a full scale of bidirectional power rating, it will lead to unnecessary cost increase of the hardware. Thus, the design objective of the ST in this article is to satisfy the asymmetrical power flow and, meanwhile, save the cost of hardware.

Based on the industrial demonstrating projects and academic research [7]–[11], the modularization is a promising solution to design the architecture of the ST (solid-state-transformer) due to the capability of fault redundancy and flexible scalability. If no real MVdc grid is needed, the cascaded H-bridge (CHB) plus a dc–dc stage can transfer the voltage from MVac to LVdc with less power semiconductors and less cost as well, as shown in Fig. 1.

Regarding the dc–dc stage, a single active bridge (SAB) [9], dual active bridge (DAB) [7], [10], SAB-based series-resonant converter (SAB-SRC) [11], and DAB-SRC are all the potential candidates. The SAB-SRC and DAB-SRC can improve the efficiency as compared to the DAB, but the DAB has better performance in terms of the dc voltage regulation, due to higher controllability. The SAB-SRC and SAB can significantly reduce the cost of power semiconductors in the secondary side but can only operate in the forward mode as compared to the DAB. The unidirectional operation cannot satisfy the reverse power operation requirement of the ST. In contrast, the DAB can flexibly operate in both directions, but leads to unnecessary cost increase of the power semiconductors due to only partial power and short period per day operating in the reverse mode.

This article proposes an asymmetrical bidirectional dc–dc (AB-DC/DC) converter. In the proposed AB-DC/DC converter, a full-scale active bridge is used in the primary side, while a partial-scale diode bridge and a partial-scale active bridge are connected in parallel in the secondary side. However, such a configuration suffers from two challenges in terms of power sharing and circulating power between the diode bridge and the partly scale active bridge in forward and reverse operation modes, respectively.

When power converters are connected in parallel, circulating currents may appear among them [12]–[16]; these were reported typically for grid-connected active inverters and active dc–dc converters in a parallel configuration, where they desire an

Manuscript received July 3, 2019; revised October 3, 2019; accepted November 18, 2019. Date of publication December 1, 2019; date of current version March 13, 2020. This work was supported by the European Research Council under the European Union's Seventh Framework Program (FP/2007-2013: Highly Efficient And Reliable smart Transformer) under Grant 616344 and by CONACyT under project No. 291626 (I0000/727/2017). Recommended for publication by Associate Editor D. Xu. *(Corresponding author: Rongwu Zhu.)*

R. Zhu, F. Hoffmann, and M. Liserre are with the Chair of Power Electronics, Kiel University, 24118 Kiel, Germany (e-mail: rzh@tf.uni-kiel.de; fho@tf.uni-kiel.de; liserre@ieee.org).

N. Vázquez is with the Department of Electronics Engineering, Instituto Tecnológico de Celaya, Celaya 38010, México (e-mail: n.vazquez@ieee.org).

K. Wang is with the Jiangsu Province Laboratory of Mining Electric and Automation and the School of Electrical and Power Engineering, China University of Mining and Technology, Xuzhou 221116, China (e-mail: kangan_wang@163.com).

Color versions of one or more of the figures in this article are available online at http://ieeexplore.ieee.org.

Digital Object Identifier 10.1109/TPEL.2019.2957407

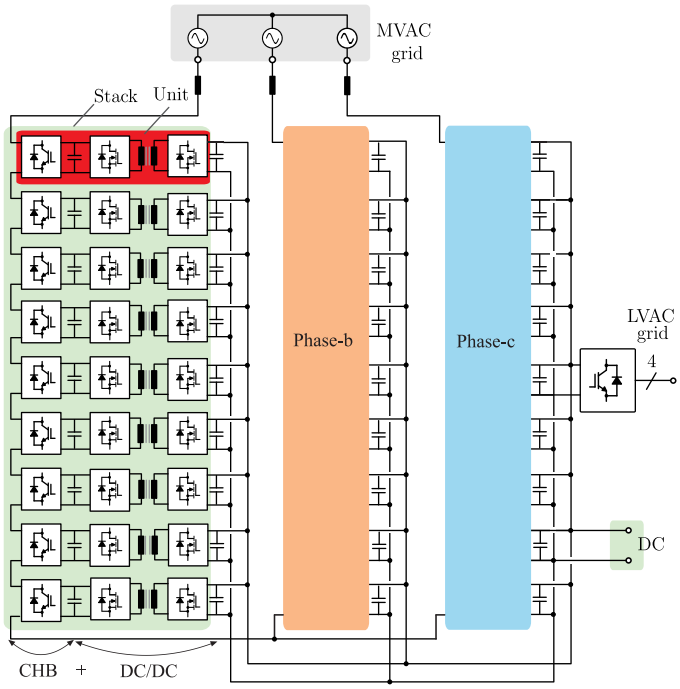


Fig. 1. Architecture of the CHB+DAB-based ST.

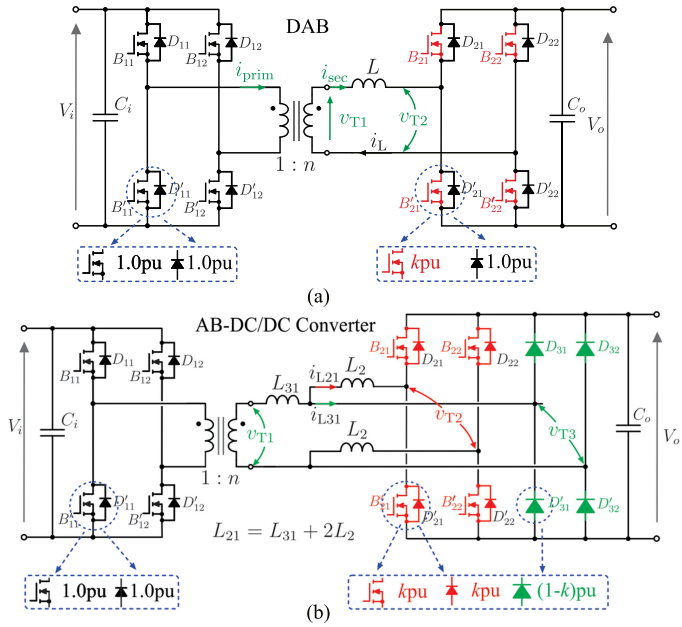


Fig. 2. Proposed AB-DC/DC converter with full-scale power in forward operation and partial-scale power in reverse operation. (a) Concept of the proposed AB-DC/DC converter. (b) Topology of the proposed AB-DC/DC converter.

equal shared power. The low-frequency component is generally caused by the injected zero-sequence component in the reference voltages to increase the dc-link voltage utilization, and the high-frequency components are caused by the asymmetrical turn-ON and turn-OFF of the power semiconductors in parallel converters in each switching period. In contrast, the proposed AB-DC/DC converter works as an SAB in the forward operation mode, and the secondary-side two bridges are equivalent as two parallel diode bridges. Due to the conduction mechanism of the diode bridge, no circulating power exists between them. In contrast, when the proposed AB-DC/DC converter works in the reverse mode, since power circulating is between an active bridge and a diode bridge, the ideas used in the aforementioned circulating suppression were based on paralleled active converters and no more suitable for the proposed AB-DC/DC converter.

Since the conventional DAB converter has only one input and one output bridge, there do not exist the aforementioned power sharing and circulating issues that aroused in the proposed converter. The DAB converter has been extensively studied in terms of efficiency optimization and dynamic improvement over the past decade [17]. The efficiency can be improved by using various modulation strategies, e.g., modulation index and phase-shift-based modulation [18], extended phase-shift modulation [19], dual phase shift [20], and triple phase shift [21] to reduce or eliminate the reactive power. The dynamic performances of the DAB are improved by either improving the modulation [22] or feeding forward load currents [23]. A voltage feedback and feedforward control was proposed to balance the dc-link voltage and power of the DAB in solid-state transformer applications [7].

Based on the operating mechanism of the AB-DC/DC converter, this article proposes effective strategies to accurately share the power in forward operation and to eliminate the power circulation in reverse operation. The rest of this article is organized as follows. Section II introduces the proposed AB-DC/DC converter topology and its forward and reverse operation modes, and as well as the comparison of cost and performance. In Section III, the power sharing design in forward operation, circulating power suppression in reverse operation, and the control scheme of the overall system are proposed. Simulation and experimental results are shown in Sections IV and V, respectively. Section VI concludes this article.

## II. Proposed AB-DC/DC Converter

### A. Topology of the Proposed AB-DC/DC Converter

The idea of the proposed AB-DC/DC converter is shown in Fig. 2. The rated power of the AB-DC/DC converter is 1.0 p.u., and the rated power of the MOSFETs in the primary-side H-bridge is 1.0 p.u. In contrast, the rated power of MOSFETs is only $k$ p.u. ($k < 1.0$), and the rated power of diodes in the secondary-side H-bridge is 1.0 p.u., as shown in Fig. 2(a). Since no existing commercial MOSFETs have different power ratings of the MOSFET and the body diode, in practice, to obtain different power ratings of the MOSFET and the diode, an extra full-bridge diode rectifier (FBDR) ($1 - k$ p.u.) is connected in parallel with a full bridge active rectifier (FBAR) ($k$ p.u.) at the secondary side, as shown in Fig. 2(b).

The operation modes of the proposed AB-DC/DC converter include forward and reverse operation modes, as shown in Fig. 3(a) and (b), respectively. Under the forward operation mode, $k$ p.u. power flows through the FBAR and $(1 - k)$ p.u. power flows through the FBDR, while under the reverse operation mode, only $k$ p.u. power flows through the FBAR.

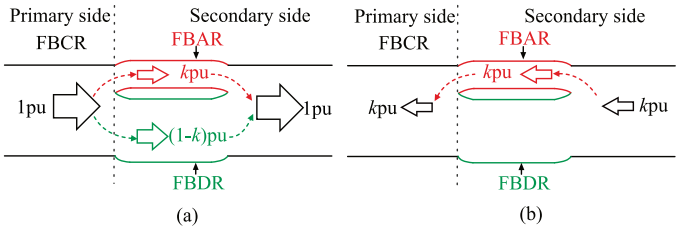


Fig. 3. Power flow in the proposed AB-DC/DC converter under (a) the forward operation mode and (b) the reverse operation mode.

TABLE I
PARAMETERS OF CREE SIC 1.2-KV DEVICES @100°

| Converter | Sic-MOSFET | | Sic-DIODE | |
|---|---|---|---|---|
| | Type | $I_d$ | Type | $I_d$ |
| DAB | C2M0025120D | 60A | - | - |
| AB-Conv.-1 | C2M0080120D | 24A | C4D30120D | 64A |
| AB-Conv.-2 | C2M0080120D | 24A | C4D10120D | 25A |

### *B. Cost Comparison of the DAB and the AB-DC/DC Converter*

In the CHB-based ST, the input and output dc-link voltages of the dc–dc converter both can be designed as 800 V [10]. Moreover, in order to reduce the power losses and increase the efficiency, wide-bandgap devices could be used instead of conventional silicon-based devices. Thus, for a 30-kW dc–dc converter module, the 1.2-kV SiC-MOSFET and the SiC diode are chosen, as shown in Table I.

Since only the secondary side of the proposed AB-DC/DC converter is different as compared to the conventional DAB, the choice of the devices only focuses on the secondary-side converters. The SiC MOSFET C2M0025120D (1.2 kV, 60 A @100°) is used as the reference device in the DAB. In the proposed AB-DC/DC converter, to obtain 0.4 p.u. reverse power capability, based on the product list of SiC devices, there are two options, e.g., SiC diode C4D30120D (64 A) used in the FBDR and C2M0080120D (24 A) used in the FBAR, named as AB-DC/DC-1; and 2xSiC diode C4D10120D (2*25 A) in parallel (50 A) used in the FBDR and SiC MOSFET C2M0080120D (24 A) used in the FBAR, called as AB-DC/DC-2.

It is very difficult to precisely estimate the cost, because the price of the power semiconductors is dependent on the market competition, distributor, and quantity acquired. As a general case, the cost of the SiC devices was obtained directly from the devices manufacture Cree Wolfspeed [24]. The power semiconductor cost of the secondary-side converter of AB-DC/DC-1 and AB-DC/DC-2 is reduced by 28% and 44%, respectively. In order to clearly show the significance of the proposed AB-DC/DC converter in hardware cost reduction, referred to [25], the detailed comparison of the CHB+DC/DC stage in a 1-MVA ST is shown in Fig. 4, where MFT is the medium-frequency transformer. The hardware cost of the DAB is about 85.78% of the CHB+DAB stage in a 1-MVA ST. AB-DC/DC-1 and AB-DC/DC-2 can reduce 8.61% and 11.3% cost of hardware as compared to the DAB converter, as shown in Fig. 4(b).

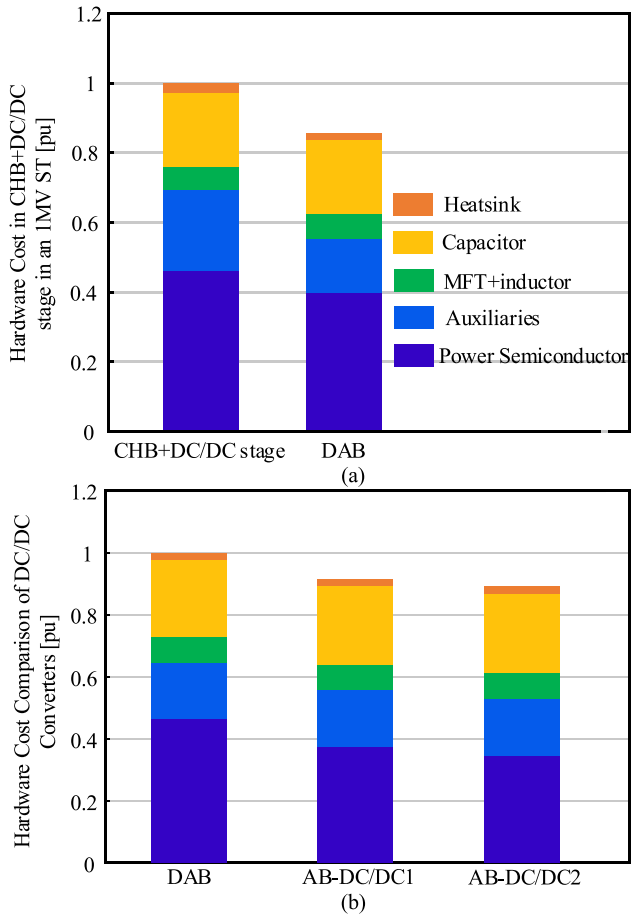


Fig. 4. Hardware cost comparison (a) between the CHB+DAB stage and the DAB and (b) among DAB, AB-DC/DC-1, and AB-DC/DC-2 in a 1-MVA ST.

TABLE II
QUALITATIVE COMPARISON OF BIDIRECTIONAL ISOLATED DC–DC CONVERTERS

| | DAB | SRC | LLC | AB-DC/DC |
|---|---|---|---|---|
| Control complexity | ++ | + | +++ | ++ |
| Current stress | + | + | + | ++ |
| Number of components | + | + | + | ++ |
| Hardware costs | ++ | ++ | ++ | + |
| Limitation in load regulation | + | +++ | ++ | + |
| Volume | + | + | ++ | ++ |

### *C. Performance Comparison*

A qualitative comparison with other commonly used soft-switching isolated bidirectional dc–dc converters is provided in Table II. In general, these converters can achieve high power density. The comparison focuses on complexity, current stresses, number of components, costs, and limitations in load regulations.

The proposed converter has two different control modes with respect to the power flow direction. Even though both control modes are easy to be implemented, the control system of the proposed converter has a slightly higher control complexity as compared to that of others, which only have one control mode.

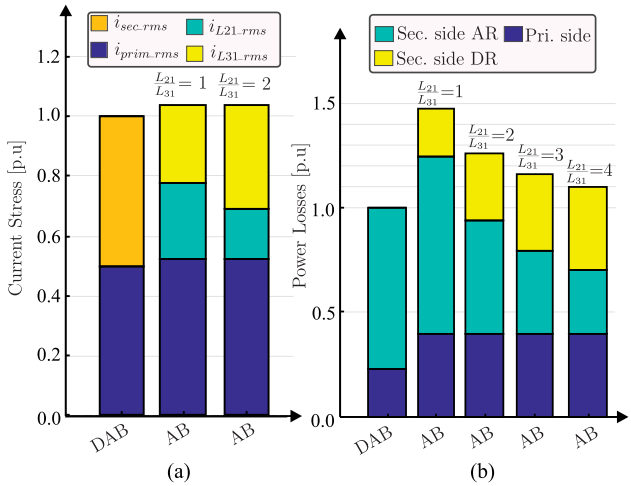


Fig. 5. Comparison of the DAB and the proposed AB-DC/DC converter in terms of (a) current stress and (b) power losses.

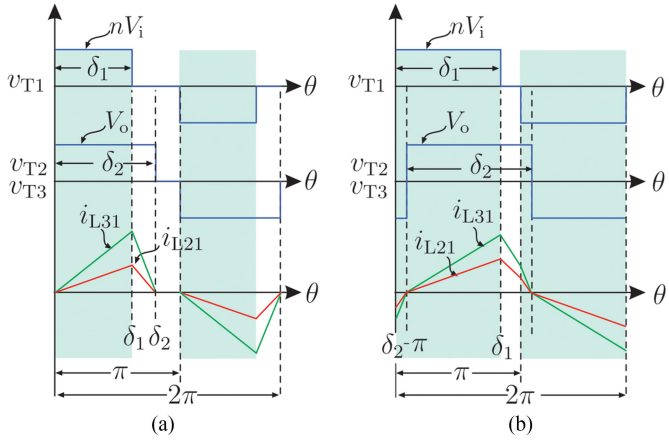


Fig. 6. Detailed waveforms of the AB-DC/DC converter working at the forward-mode (a) discontinuous current and (b) continuous current.

Resonant converters, such as the LLC and the SRC, show best performance with frequency control (50% duty cycle). However, the operation across a wide frequency range leads to a complex optimization procedure in the converter design (e.g., filter design). The compared topologies are voltage-sourced topologies. The absence of an input filter in the topologies leads to similar input voltage ripples. Due to the similar operation principle between the AB-DC/DC and the DAB, the resulting voltage spikes are comparable.

Furthermore, a detailed comparison with the DAB is provided in Fig. 5. The transformer rms currents, which give insight about the device current stresses, are evaluated, as shown in Fig. 5(a). In comparison, the current stress is about 3.6% higher in the proposed AB-DC/DC converter as compared to the DAB converter. The power losses are also higher than the DAB converter, but with increasing the inductance ratio, $L_{21}/L_{31}$, from 1 up to 4, the power losses can be reduced from 1.47 to 1.26, 1.16, and 1.09 p.u., as shown in Fig. 5(b).

## III. Control Strategy of the Proposed AB-DC/DC Converter

As analyzed above, the proposed AB-DC/DC converter can effectively save the cost. However, two corresponding issues need to be solved, e.g., how to share the power in the forward operation mode and to suppress the power circulation between two parallel full bridges under the reverse operation mode.

### A. Power Sharing Under the Forward Operation Mode

Under the forward operation mode, the FBAR in the secondary side is turned OFF and then operates as an FBDR as well. Consequently, the secondary side of the AB-DC/DC converter can be equivalent as two FBDRs connected in parallel, as shown in Fig. 2(b), and the power sharing between the two FBDRs needs to be properly designed avoiding damaging power semiconductors, as shown in Fig. 3(a).

Under the forward operation mode, to operate properly, the converter input bridge is controlled by means of $\delta_1$, determined by the working conditions, and the detailed ideal waveforms of the AB-DC/DC converter are shown in Fig. 6, where $v_{T1}$, $v_{T2}$, and $v_{T3}$ are the terminal voltages at the transformer secondary side, the leg voltage of the FBAR, and the leg voltage of the FBDR, respectively, as shown in Fig. 2(b).

Based on Fig. 6, the quantitative calculation of inductor currents in the secondary side of the AB-DC/DC converter under current discontinuous and continuous conditions can be expressed as (1) and (2), respectively. It is noted that, in practice, voltage oscillation may appear when ac is equal to zero under current discontinuous mode due to the parasitic elements

$$i_{L21}(\theta)=\begin{cases}\dfrac{nV_i-V_o}{\omega L_{21}}\theta, & 0<\theta\le\delta_1\\ \dfrac{nV_i-V_o}{\omega L_{21}}\delta_1-\dfrac{V_o}{\omega L_{21}}(\theta-\delta_1), & \delta_1<\theta\le\delta_2\\ 0, & \delta_2<\theta\le\pi\end{cases}\tag{1}$$

$$i_{L21}(\theta)=\begin{cases}\dfrac{nV_i+V_o}{\omega L_{21}}\theta+i_{L21}(0), & 0<\theta\le\delta_2-\pi\\ \dfrac{nV_i-V_o}{\omega L_{21}}(\theta-\pi+\delta_2), & \delta_2-\pi<\theta\le\delta_1\\ i_{L21}(\delta_1)-\dfrac{V_o}{\omega L_{21}}(\theta-\delta_1), & \delta_1<\theta\le\pi\end{cases}\tag{2}$$

where $L_{21}=L_{31}+2L_2$.

According to the voltage and second balance theory, as shown in Fig. 6, the relationship between the voltages and duty cycles can be obtained as

$$nV_i\delta_1=V_o\delta_2.\tag{3}$$

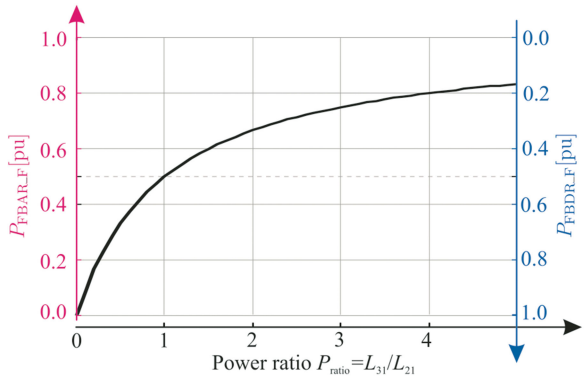


Fig. 7. Profile of power sharing in the forward operation mode.

Based on Fig. 6, the average active power flowing through the FBAR, as shown in Fig. 3(a), can be obtained as

$$P_{\mathrm{FBAR\_F}} = \frac{1}{\pi}\left(\int_0^{\delta_1} v_{\mathrm{T2}} i_{\mathrm{L21}}(\theta)d\theta + \int_{\delta_1}^{\delta_2} v_{\mathrm{T2}} i_{\mathrm{L21}}(\theta)d\theta\right). \tag{4}$$

By substituting (1) into (4), the power flowing through the FBAR can be obtained as

$$P_{\mathrm{FBAR\_F}} = \frac{nV_{\mathrm{i}}V_{\mathrm{o}}}{2\pi\omega L_{21}}\delta_1^2\left(\frac{nV_{\mathrm{i}}}{V_{\mathrm{o}}} - 1\right). \tag{5}$$

Similarly, the current in the FBDR, $i_{\mathrm{L31}}$, can be easily obtained by replacing $L_{21}$ with $L_{31}$ in (1) and (2), respectively, and then, the power flowing through the FBDR can be obtained as

$$P_{\mathrm{FBDR\_F}} = \frac{nV_{\mathrm{i}}V_{\mathrm{o}}}{2\pi\omega L_{31}}\delta_1^2\left(\frac{nV_{\mathrm{i}}}{V_{\mathrm{o}}} - 1\right). \tag{6}$$

Based on (5) and (6), the power sharing ratio between the FBAR and the FBDR is determined by the inductance ratio, $L_{21}$ and $L_{31}$, directly, as follows:

$$P_{\mathrm{ratio}} = \frac{P_{\mathrm{FBAR\_F}}}{P_{\mathrm{FBDR\_F}}} = \frac{L_{31}}{L_{21}}. \tag{7}$$

Based on (7), the relationship of the power sharing between the FBAR and the FBDR is clearly shown in Fig. 7. The power sharing between the FBDR and the FBAR can be accurately achieved by changing the ratio of the inductance. Then, to get a constant output power, the angle $\delta_1$ is calculated accordingly with (5). As can be observed, zero in the ratio $L_{31}/L_{21}$ leads to more power in the FBDR. When the ratio is increased more power goes through FBAR. The power is equally shared when the ratio is equal to 1; this means that both inductances are equal.

### *B. Circulating Power Suppression Under the Reverse Operation Mode*

When the proposed AB-DC/DC converter operates in the reverse mode, the FBDR is blocked due to the limited capability of unidirectional power flow and the FBAR works as an active bridge instead of a diode bridge in the forward operation mode.

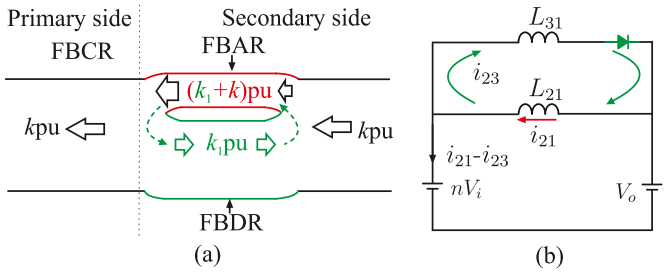


Fig. 8. (a) Circulating power flow and (b) equivalent circuit of circulating power under the reverse operation mode.

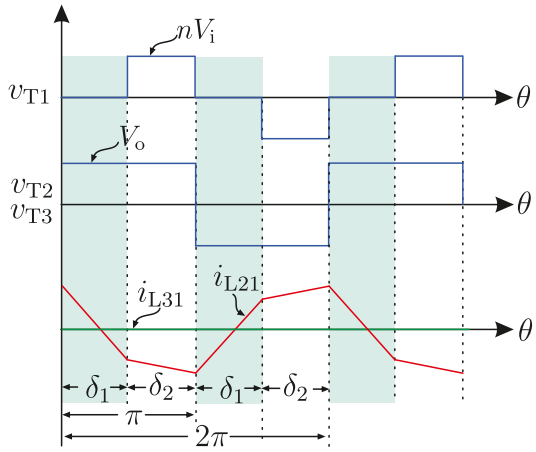


Fig. 9. Detailed waveforms of the AB-DC/DC converter working at the reverse mode.

In the reverse mode, it is important to consider how to avoid the circulating power between the FBAR and the FBDR in the secondary side, as shown in Fig. 8(a), and its equivalent circuit is shown in Fig. 8(b), including two inductors, voltage at the secondary side of the transformer terminal, $v_{\mathrm{T1}}$ ($nV_{\mathrm{i}}$), output voltage ($V_{\mathrm{o}}$), and a diode used to represent the diode bridge in the FBDR. If the voltage of $v_{\mathrm{T1}}$ is positive and higher than $v_{\mathrm{o}}$, then the diode rectifier will conduct leading circulating current, $i_{23}$. In order to eliminate this current, it must be ensured that the FBDR will not conduct, and an effective way is to keep the output voltage higher than $nV_{\mathrm{i}}$, i.e.,

$$nV_{\mathrm{i}} < V_{\mathrm{o}}. \tag{8}$$

Then, according to this operation, steady-state waveforms of the proposed AB-DC/DC converter, in the reverse mode, are shown in Fig. 9, where a duty-cycle-based control is adopted to easily reduce the switching losses. Now, the FBDR is disabled; this means that no current flows through it, and this is because the output voltage is increased to avoid the circulating power. In this mode, the proposed AB-DC/DC converter is working as a conventional DAB, and the active bridge in the primary side is controlled by means of $\delta_1$.

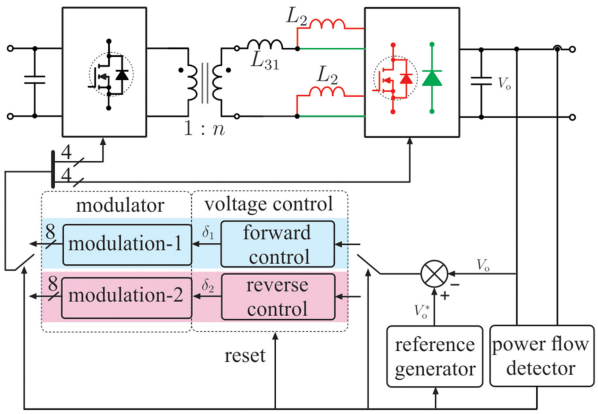


Fig. 10. Control block diagram of the proposed dc–dc converter.

At the steady state, inductor currents in the reverse operation mode are described by

$$i_{\mathrm{L21}}(\theta) = \begin{cases} -\dfrac{V_\mathrm{o}}{\omega L_{21}}\theta + i_0, & 0 < \theta \le \delta_1 \\ \dfrac{nV_\mathrm{i} - V_\mathrm{o}}{\omega L_{21}}(\theta - \delta_1) - \dfrac{V_\mathrm{o}}{\omega L_{21}}\delta_1 + i_0, & \delta_1 < \theta \le \pi \end{cases} \tag{9}$$

where $i_0$ is the initial current, and $\delta_1 + \delta_2 = \pi$.

Since the current is symmetrical in $\pi$, the initial current $i_0$ can be obtained as

$$i_0 = \frac{1}{2\omega L_{21}}\left(V_\mathrm{o}\pi - nV_\mathrm{i}\delta_2\right). \tag{10}$$

Based on (9) and (10), the power flowing through the FBAR in the reverse operation mode can be obtained as

$$P_{\mathrm{FBAR\_R}} = -\frac{nV_\mathrm{i}V_\mathrm{o}}{2\omega L_{21}}\delta_2\left(1 - \frac{\delta_2}{\pi}\right). \tag{11}$$

The negative sign in (11) means that the power is going in the reverse mode.

### C. Control System Description of the Proposed AB-DC/DC Converter

Based on (5), (6), and (11), it clearly shows that under the forward operation mode, the duty cycle, $\delta_1, (0 \le \delta_1 \le \pi/2)$, based voltage control can be used, while under the reverse operation mode, the duty cycle, $\delta_2, (-\pi/2 \le \delta_2 \le 0)$ based voltage control can be adopted. The details of the modulated voltage waveform under forward and reverse operation modes are shown in Figs. 6 and 9, respectively.

The control block diagram of the proposed AB-DC/DC converter is shown in Fig. 10. Based on the direction of power flow, a flag signal is generated to enable switching the voltage control mode, as well as voltage reference between the forward and reverse control. It is noticed that the integrator in the voltage controller needs to be reset when the control mode is changed. The dynamic performances of voltage control during working mode switching is different because the converter can provide the rated power to response the change of voltage setpoint when switching from the reverse mode to the forward mode, while from the forward mode to the reverse mode, the dynamic response of voltage control is mainly determined by the amount of reverse power.

TABLE III
SIMULATION SYSTEM PARAMETERS

| Parameters | Symbols | Value |
|---|---|---|
| Input DC voltage(V) | $V_\mathrm{i}$ | 200 |
| Inductance at FBDR($\mu$H) | $L_{31}$ | 40 |
| Inductance at FBAR($\mu$H) | $L_{21}$ | 80 |
| Switching frequency(kHz) | $f_\mathrm{s}$ | 20 |
| Output capacitance($\mu$F) | $C_\mathrm{o}$ | 250 |
| Transformer turn ratio($N_1/N_2$) | $N_{12}$ | 1:1 |
| Rated power at forward mode(W) | $P_{\mathrm{FM}}$ | 1000 |
| Rated power at reverse mode(W) | $P_{\mathrm{RM}}$ | -333 |
| Output voltage at forward mode(V) | $V_\mathrm{o}$ | 180 |
| Output voltage at reverse mode(V) | $V_\mathrm{o}$ | 220 |

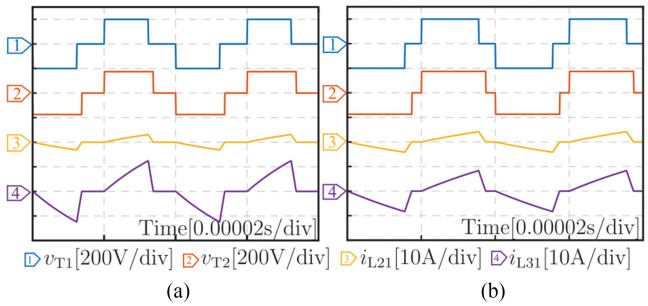


Fig. 11. Simulation results of the impacts of the inductance ratio on power sharing under the forward operation mode with (a) $L_{21}/L_{31} = 2$, ($L_{31} = 40\,\mu$H and $L_{21} = 80\,\mu$H) and (b) $L_{21}/L_{31} = 4$ ($L_{31} = 20\,\mu$H and $L_{21} = 80\,\mu$H).

## IV. Simulation Results

The proposed AB-DC/DC converter was designed and numerically simulated. The simulation parameters are summarized in Table III, and the system configuration is the same as in Fig. 2(b).

### A. Power Sharing Under the Forward Operation Mode

The results obtained in the forward operation mode are shown in Fig. 11, where the output voltage, inductor currents, and voltages $v_{\mathrm{T1}}$ and $v_{\mathrm{T2}}$ are shown. The output dc voltage is regulated at 180 V.

When the power sharing ratio is $L_{21}/L_{31} = 2$, which means that the FBDR handles twice of the power than the FBAR, the current $i_{\mathrm{L31}}$ is double of $i_{\mathrm{L21}}$, which confirms that the FBDR handles double power, as shown in Fig. 11(a). The voltage waveforms of the bridges ($v_{\mathrm{T1}}$ and $v_{\mathrm{T2}}$) are in good agreement with the theory.

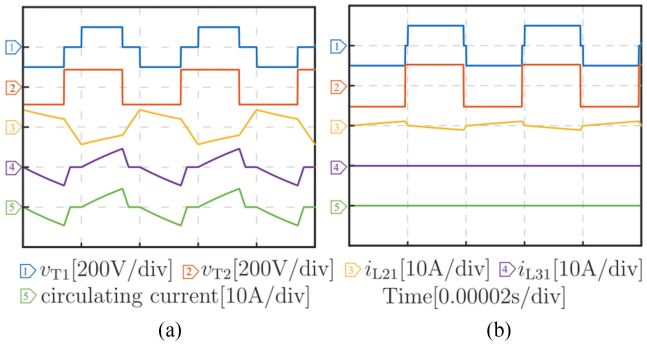


Fig. 12. Simulation results of the proposed AB-DC/DC converter under the reverse operation mode (a) without and (b) with the proposed circulating power suppression.

Fig. 11(b) shows the operation of the proposed AB-DC/DC converter but considering a different inductance ratio. In this case, the ratio is 4; then, the FBDR handled four times energy of the FBAR in the forward operation mode; the inductor $L_{31}$ has been reduced to 20 $\mu$H. As can be observed, the current of the FBDR is increased, and the FBAR current is reduced. The output power is the same as the case of in Fig. 11(a); then, clearly, it can be observed how the power is shared in a controlled manner.

### *B. Circulating Power Suppression Under the Reverse Operation Mode*

The simulation results under the reverse operation mode are shown in Fig. 12. Fig. 12(a) shows the operation of the system not satisfying (8); for this, $V_o$ is set to 180 V, which is the same as in the forward operation mode; then, a circulating power appears between the FBDR and FBAR, but this power does not go to the primary side, leading extra power losses and potentially destroying the power semiconductors. As can be observed, the circulating current increases the amplitude of $i_{L21}$ and $i_{L31}$. Also, it must be noted that, in order to compensate for the power flow in the FBDR, the active bridge handles more power than required (see the current level).

To avoid this, the converter must be operated satisfying (8) and then operated as in Fig. 12(b). Compared to Fig. 12(a), the circulating current is reduced to 0 A; the amplitude of $i_{L31}$ is 0 A and that of $i_{L21}$ is significantly reduced. The output voltage is regulated to 210 V, which can effectively avoid the circulating current between the FBDR and the FBAR in the secondary side. Again, voltage waveforms of the bridges ($v_{T1}$ and $v_{T2}$) are in good agreement with the theory.

### *C. Transient Performances*

The results under transition are shown in Fig. 13. The proposed control strategy can fast change from one operation mode to another in 0.004 s. From forward operation to reverse operation, with the increase of the output voltage, $v_o$, from 180 to 210 V, the current in the FBDR, $i_{L31}$, fast decreases to zero and only the FBAR works, as shown in Fig. 13(a). On the other hand, when the operation mode changes from reverse to forward operation, the output voltage $v_o$ is reduced from 210 to 180 V, and then, currents in the FBAR and the FBDR are properly shared, as shown in Fig. 13(b).

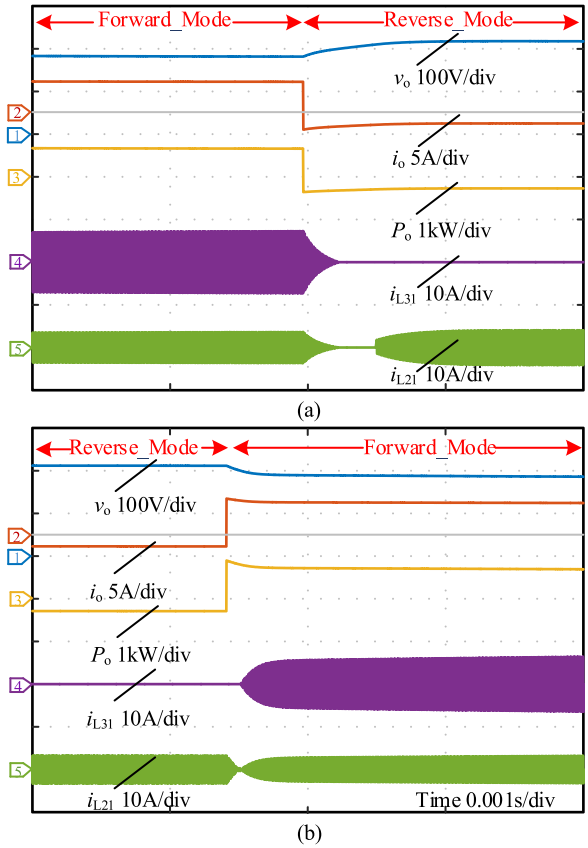


Fig. 13. Simulation results of transitions (a) from the forward operation mode to the reverse operation mode and (b) from the reverse operation mode to the forward operation mode.

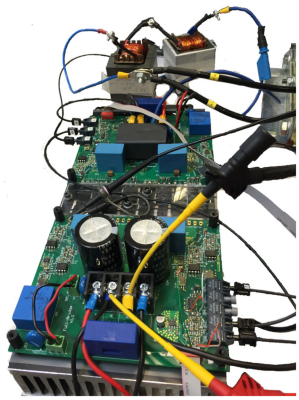

Fig. 14. Photograph of the experimental prototype.

## V. Experimental Results

A 1-kW experimental prototype was designed and built in the laboratory, with the photograph as shown in Fig. 14. The converter consists of three bridges, as shown in Fig. 2(b), two active bridges, and one diode bridge. Different tests were carried out to illustrate the effective operation of the proposal.

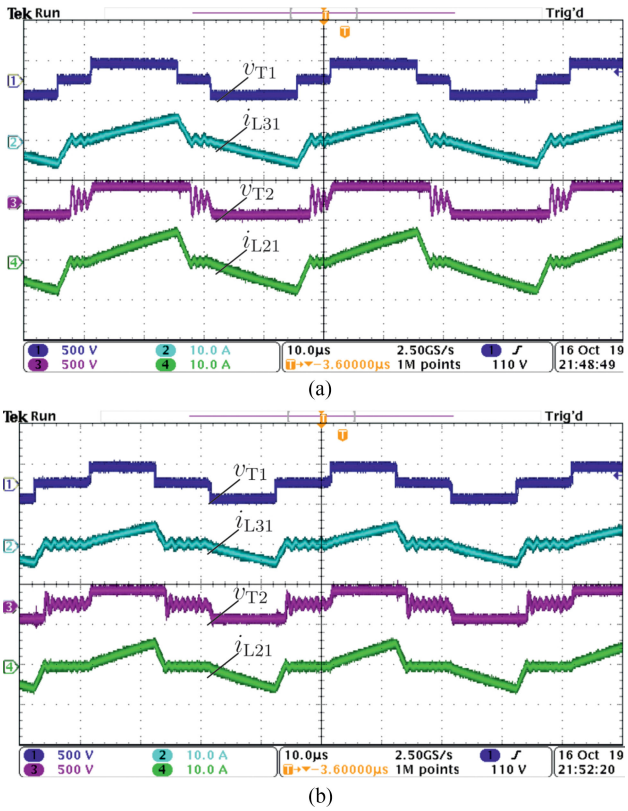


Fig. 15. Experimental results of the proposed converter under the forward operation mode with (a) 1-kW and (b) 0.6-kW power ($L_{21} = L_{31} = 40\,\mu$H).

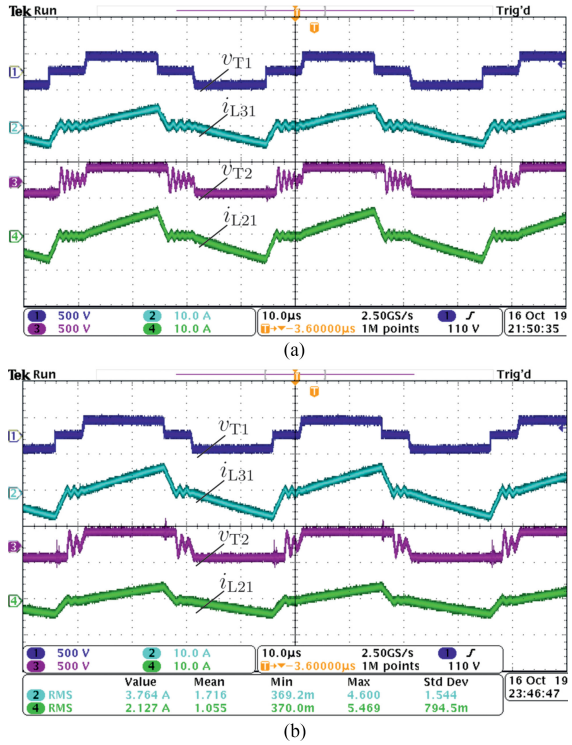


Fig. 16. Experimental results of power sharing under the forward operation mode with 0.8-kW power. (a) $L_{21} = L_{31} = 40\,\mu$H. (b) $L_{21} = 80\,\mu$H and $L_{31} = 40\,\mu$H.

### A. *Forward Operation Mode*

The experimental results of the proposed AB-DC/DC converter working at various load conditions with the same power sharing ratio are shown in Fig. 15, where $L_{21} = L_{31} = 40\,\mu$H. The power is 1 kW in Fig. 15(a) and 0.6 kW in Fig. 15(b). In these two cases, the current ratio between the FBAR and the FBDR ($i_{L21}$ and $i_{L31}$) in Fig. 15(a) and (b) is almost the same, i.e., 1:1 with slightly deviation, due to the measured error of inductances. Thus, Fig. 15 validates that the AB-DC/DC converter can work properly with various load conditions when the power sharing ratio is fixed.

The experimental results of the AB-DC/DC converter power sharing capability are shown in Fig. 16, where $L_{21} = L_{31} = 40\,\mu$H in Fig. 16(a) and $L_{21} = 80\,\mu$H and $L_{31} = 40\,\mu$H in Fig. 16(b). It can be seen that the current of the FBAR and the FBDR is almost the same, i.e., 1:1, as shown in Fig. 16(a), while the FBDR current is about two times of the FBAR current, i.e., 2:1, as shown in Fig. 16(b). The experimental results in Fig. 16 match well with simulation results in Fig. 11(a) and theoretical analysis in Fig. 7.

### B. *Reverse Operation Mode*

Under the reverse operation mode, the experimental results of circulating power suppression when the power sharing ratio is different are shown in Figs. 17 and 18, where the power

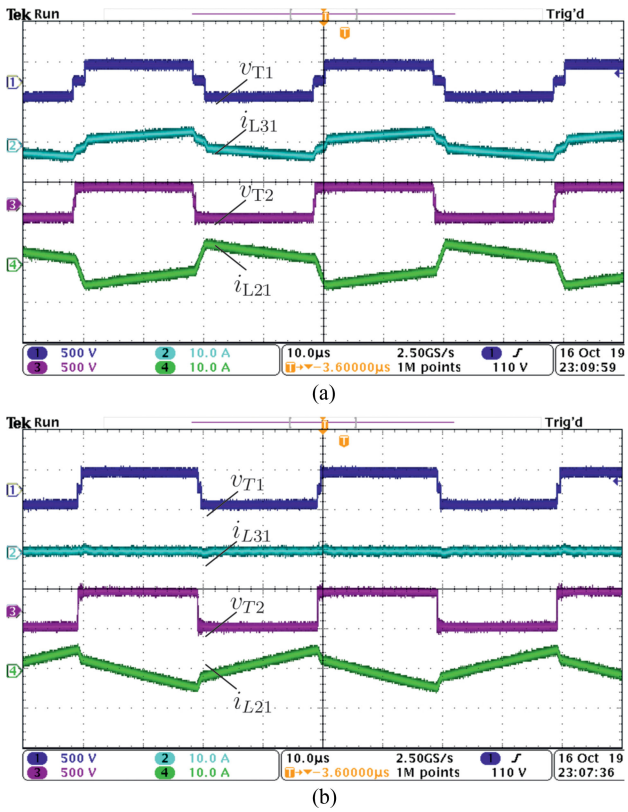


Fig. 17. Experimental results of circulating power suppression under the reverse operation mode with 0.3-kW power (a) without and (b) with the proposed control, when $L_{21} = L_{31} = 40\,\mu$H.

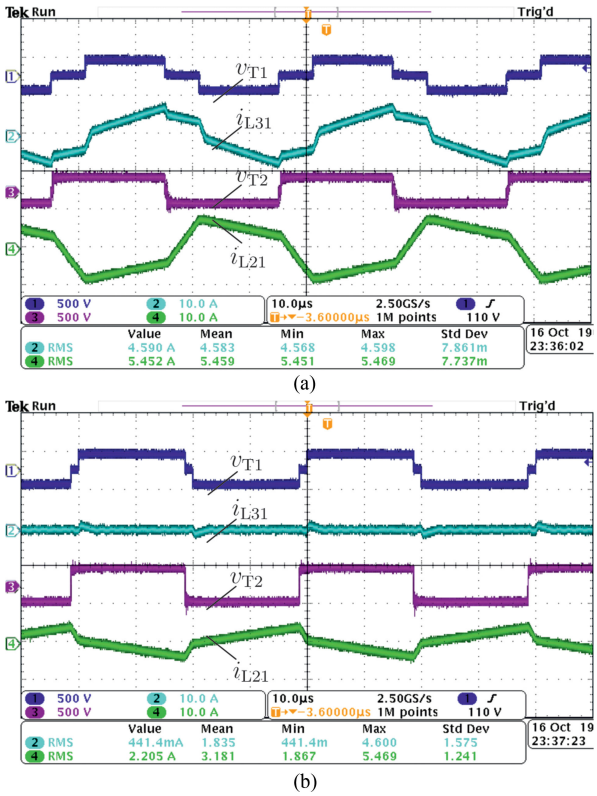


Fig. 18. Experimental results of circulating power suppression with 0.3-kW reverse power (a) without and (b) with the proposed control, when $L_{21} = 80\,\mu$H and $L_{31} = 40\,\mu$H.

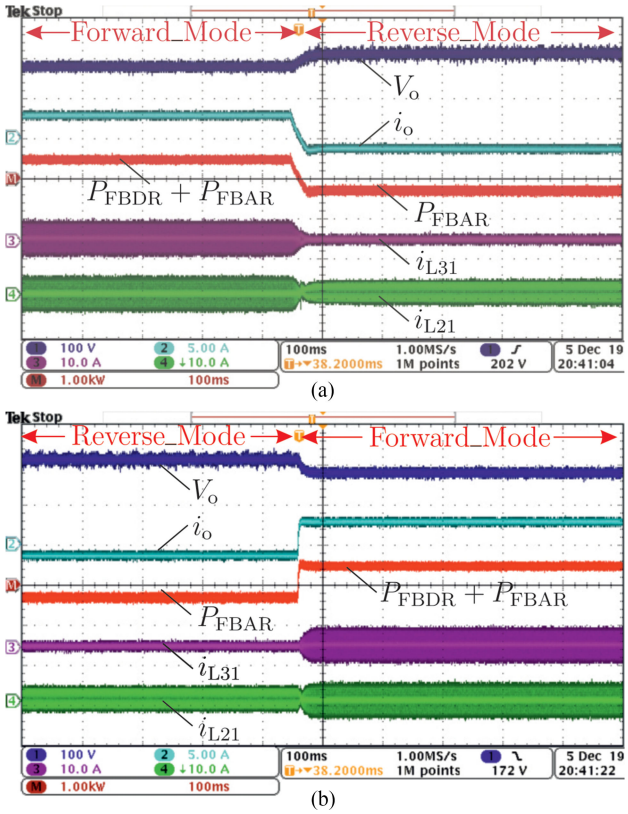


Fig. 19. Experimental results of dynamic performances. (a) Change from the forward operation mode to the reverse operation mode. (b) change from the reverse operation mode to the forward operation mode.

sharing ratio between the FBDR and the FBAR is 1:1 and 2:1, respectively.

As shown in Fig. 17(a), without the proposed circulating power suppression, the directions of the FBDR current $i_{L31}$ and the FBAR current $i_{L21}$ are opposite, indicating power circulation between the FBAR and the FBDR, and the circulating current is equal to $i_{L31}$. In contrast, with the proposed control, the FBDR current $i_{L31}$ is completely suppressed to zero, which means the circulating current is zero as well, and thus, no power circulates between them. Similar to Fig. 17, the experimental results in Fig. 18 clearly show that the proposed control can effectively suppress the circulating power under the reverse operation mode, and the FBAR current $i_{L21}$ is smaller than no circulating power suppression. The results in Figs. 17 and 18 both validate the correctness of the theoretical analysis and the simulation results in Fig. 10.

As shown in Figs. 17(a) and 18(a), when the FBAR inductance $L_{21}$ is increased from 40 to $80\,\mu$H, the circulating power is increased dramatically, which will significantly increase the power losses and reduce system efficiency. Moreover, the uncontrolled circulating power will lead to overloading of the FBAR. Therefore, the proposed power circulating suppression solution has more contribution when the power sharing ratio is different.

### C. Dynamic Performances and Efficiency

The dynamic performances of the proposed AB-DC/DC converter are shown in Fig. 19. In Fig. 19(a), the output power is 500 W at the forward operation mode, and the ac current in the FBDR and the FBAR is equal, and then, due to the reverse power ($-300$ W), the output dc-link voltage arises from 180 to 210 V, the ac current in the FBDR, $i_{L31}$, reduces to zero, and all the power goes through the FBRA. In contrast, when the power increases from $-300$ to 500 W, the output dc-link voltage $V_o$ decreases from 210 to 180 V, and the FBDR current $i_{L31}$ increases from zero to be equal to the FBAR current $i_{L21}$, as shown in Fig. 19(b). The experimental results in Fig. 19 clearly validate that the proposed control can effectively switch between two operation modes.

Operating efficiency under different load conditions and operating modes is compared in Fig. 20. When the proposed converter works in the reverse mode, the circulating power leads to high power losses in the FBAR and the FBDR, and thus, the efficiency is lower. In contrast, the proposed power circulating power sharing method can effectively improve system efficiency, as shown in Fig. 20(a). The impact of the power sharing ratio under forward operation mode is shown in Fig. 20(b). When $P_{FBDR}/P_{FBAR} = 1{:}1$, the efficiency is lower than that of $P_{FBDR}/P_{FBAR} = 2{:}1$, due to high current flowing through the body diode of the MOSFET and the body diode, which have worse performances, in the active bridge, as compared to the extra SiC diode. The efficiency of the DAB is higher when the operating power is higher than 0.3 p.u., while the

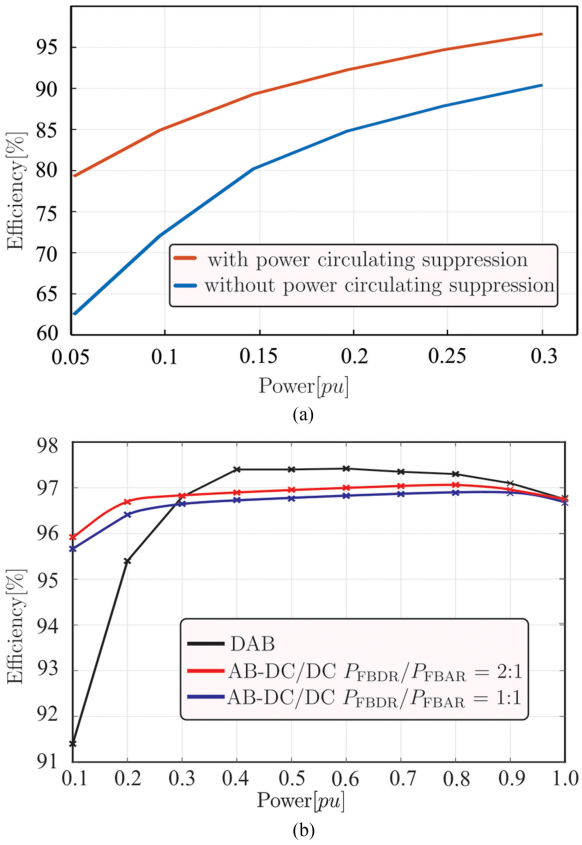


Fig. 20. Experimental results of efficiency comparison of dc–dc converters. (a) Efficiency at the reverse mode with and without power circulating suppression. (b) Efficiency at the forward operation mode with the power sharing ratio $P_{\mathrm{FBDR}}/P_{\mathrm{FBAR}}$ = 1:1 and 2:1.

proposed AB-DC/DC converter can obtain higher efficiency when operating at a low power range.

## VI. Conclusion

In this article, an AB-DC/DC converter is proposed for the ST to deal with the asymmetrically bidirectional power flow, where the forward power flow can reach 1.0 p.u., but the reverse power is partial only. Compared to the conventional DAB converter, the proposed one can save about 44% cost of the power semiconductor devices in the secondary side converter and 9.7% in the overall system as compared to the full-DAB-based solution. The control strategies for two operation modes of forward operation and reverse operation have been proposed to effectively share power and suppress the power circulating between the FBAR and the FBDR in the secondary side of the proposed AB-DC/DC converter. The power sharing ratio can be easily selected by changing the inductance ratio. The power circulation can be effectively suppressed by adjusting the output voltage amplitude without any extra hardware. The maximum efficiency can reach about 97% under both operation modes. The simulation and experimental results both clearly validate the correctness and effectiveness of the proposed strategies and theoretical analyses.

## References

[1] *LV-Engine website*, 2017. [Online]. Available: https://www.spenergynetworks.co.uk/pages/ lv_engine.aspx
[2] C. Kumar, R. Zhu, G. Buticchi, and M. Liserre, "Sizing and SOC-management of a smart transformer-based energy storage system," *IEEE Trans. Ind. Electron.*, vol. 65, no. 8, pp. 6709–6718, Aug. 2018.
[3] R. Zhu, G. Buticchi, and M. Liserre, "Investigation on common mode voltage suppression in smart transformer-fed distributed hybrid grids," *IEEE Trans. Power Electron.*, vol. 33, no. 10, pp. 8438–8448, Oct. 2018.
[4] H. Mortazavi, H. Mehrjerdi, M. Saad, S. Lefebvre, D. Asber, and L. Lenoir, "A monitoring technique for reversed power flow detection with high PV penetration level," *IEEE Trans. Smart Grid*, vol. 6, no. 5, pp. 2221–2232, Dec. 2015.
[5] V. Kekatos, G. Wang, A. Conejo, and G. Giannkis, "Stochastic reactive power management in microgrids with renewables," *IEEE Trans. Power Sys.*, vol. 30, no. 6, pp. 3386–3395, Nov. 2015.
[6] G. De Carne, G. Buticchi, Z. Zou, and M. Liserre, "Reverse power flow control in a ST-fed distribution grid," *IEEE Trans. Smart Grid*, vol. 9, no. 4, pp. 3811–3819, Jul. 2018.
[7] J. Shi, W. Gou, H. Yuan, T. Zhao, and A. Q. Huang, "Research on voltage and power balance control for cascaded modular solid-state transformer," *IEEE Trans. Power Electron.*, vol. 26, no. 4, pp. 1154–1166, Apr. 2011.
[8] D. Dujic *et al.*, "Power electronic traction transformer-low voltage prototype," *IEEE Trans. Power Electron.*, vol. 28, no. 12, pp. 5522–5534, Dec. 2013.
[9] D. Rothmund, G. Ortiz, and J. W. Kolar, "SiC-based unidirectional solid-state transformer concepts for directly interfacing 400 V dc to medium-voltage ac distribution systems," in *Proc. IEEE 36th Int. Telecommun. Energy Conf.*, Sep. 2014, pp. 1–9.
[10] X. She, A. Q. Huang, and R. Burgos, "Review of solid-state transformer technologies and their application in power distribution systems," *IEEE J. Emerg. Sel. Topics Power Electron.*, vol. 1, no. 3, pp. 186–198, Sep. 2013.
[11] L. Costa, G. Buticchi, and M. Liserre, "Highly efficient and reliable SiC-based dc-dc converter for smart transformer," *IEEE Trans. Ind. Electron.*, vol. 64, no. 10, pp. 8383–8392, Oct. 2017.
[12] Y. Xia, M. Yu, Y. Peng, and W. Wei, "Modeling and analysis of circulating currents among input-parallel output-parallel nonisolated converters," *IEEE Trans. Power Electron.*, vol. 33, no. 10, pp. 8412–8426, Oct. 2018.
[13] Y. Xia, W. Wei, Y. Peng, P. Yang, and M. Yu, "Decentralized coordination control for parallel bidirectional power converters in a grid-connected dc microgrid," *IEEE Trans. Smart Grid*, vol. 9, no. 6, pp. 6850–6861, Nov. 2018.
[14] W. Jiang, Y. Gao, B. Xiao, J. Wang, X. Ding, and L. Wang, "Suppression of high-frequency circulating current caused by asynchronous carriers for parallel three-phase grid-connected converters," *IEEE Trans. Ind. Electron.*, vol. 65, no. 2, pp. 1031–1040, Feb. 2018.
[15] R. Zhu, M. Liserre, Z. Chen, and X. Wu, "Zero-sequence voltage modulation strategy for multiparallel converters circulating current suppression," *IEEE Trans. Ind. Electron.*, vol. 64, no. 3, pp. 1841–1852, Mar. 2017.
[16] Y. Xia, Y. Li, Y. Peng, M. Yu, and W. Wei, "Circulating currents suppression based on two degrees of freedom control in dc distribution networks," *IEEE Trans. Power Electron.*, vol. 33, no. 12, pp. 10815–10825, Dec. 2018.
[17] N. Hou and Y. Li, "Overview and comparison of modulation and control strategies for non-resonant single-phase dual-active-bridge dc-dc converter," *IEEE Trans. Power Electron.*, to be published.
[18] G. Oggier, G. O. GarcÃa, and A. R. Oliva, "Modulation strategy to operate the dual active bridge dc-dc converter under soft switching in the whole operating range," *IEEE Trans. Power Electron.*, vol. 26, no. 4, pp. 1228–1236, Apr. 2011.
[19] B. Zhao, Q. Yu, and W. Sun, "Extended-phase-shift control of isolated bidirectional dc-dc converter for power distribution in microgrid," *IEEE Trans. Power Electron.*, vol. 27, no. 11, pp. 4667–4680, Nov. 2012.
[20] H. Bai and C. Mi, "Eliminate reactive power and increase system efficiency of isolated bidirectional dual-active-bridge dc-dc converters using novel dual-phase-shift control," *IEEE Trans. Power Electron.*, vol. 23, no. 6, pp. 2905–2914, Nov. 2008.
[21] A. Tong, L. Hang, G. Li, X. Jiang, and S. Gao, "Modeling and analysis of a dual-active-bridge-isolated bidirectional dc/dc converter to minimize rms current with whole operating range," *IEEE Trans. Power Electron.*, vol. 33, no. 6, pp. 5302–5316, Jun. 2018.
[22] S. Lin, X. Li, C. Sun, and Y. Tang, "Fast transient control for power adjustment in a dual-active-bridge converter," *Electron. Lett.*, vol. 53, no. 16, pp. 1130–1132, 2017.

[23] J. Ge, Z. Zhao, L. Yuan, and T. Lu, "Energy feed-forward and direct feed-forward control for solid-state transformer," *IEEE Trans. Power Electron.*, vol. 30, no. 8, pp. 4042–4047, Aug. 2015.
[24] *Cree wolfspeed*. Accessed: Jun. 2019. [Online]. Available: http://www.wolfspeed.com/rf
[25] L. F. Costa, F. Hoffmann, G. Buticchi, and M. Liserre, "Comparative analysis of multiple active bridge converters configurations in modular smart transformer," *IEEE Trans. Ind. Electron.*, vol. 66, no. 1, pp. 191–202, Jan. 2019.

**Rongwu Zhu** (S'12–M'15) received the B.Eng. degree in electrical engineering from Nanjing Normal University, Nanjing, China, in 2007 and the Ph.D. degree in energy technology from Aalborg University, Aalborg, Denmark, in 2015.

He is currently a Senior Researcher with the Chair of Power Electronics, Christian-Albrechts University of Kiel, Kiel, Germany. From 2011 to 2012, he was a Guest Researcher with Aalborg University, Aalborg, Denmark. He has authored or coauthored about 80 technical papers (more than 30 of them in international peer-reviewed journals). His research interests include renewable power generation, operation and control of electric grids with high penetration of renewables, and reliability and resilience of power-electronics-dominated grids.

**Felix Hoffmann** (S'18) received the B.Sc. and M.Sc. degrees in electrical engineering and business administration in 2014 and 2016, respectively, from the Christian-Albrechts-Universität zu Kiel, Kiel, Germany, where he is working toward the Ph.D. degree with the Chair of Power Electronics.

His current research interests include high-power converters and the ultilization of wide-bandgap semiconductors.

**Nimrod Vázquez** (M'98–SM'11) was born in México City, México, in 1973. He received the B.S. degree from the Instituto Tecnológico de Celaya, Celaya, México, in 1994, and the M.Sc. and Dr. degrees from the Centro Nacional de Investigación y Desarrollo Tecnológico, Cuernavaca, México, in 1997 and 2003, respectively, all in electronics engineering.

Since 1998, he has been with the Department of the Electronics Engineering, Instituto Tecnológico de Celaya. His research interests include dc–ac converters, power factor correction, nonlinear control techniques, and renewable energy.

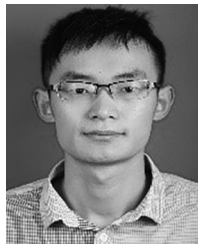

**Kangan Wang** was born in Jiangsu, China, on June 5, 1990. He received the B.S. degree in electrical engineering, in 2013 from the China University of Mining and Technology, Xuzhou, China, where he is working toward the Ph.D. degree in electrical engineering.

He was a visiting Ph.D. student with the Chair of Power Electronics, Christian-Albrechts-Universität zu Kiel, Kiel, Germany, from October 2017 to October 2019. His research interests include cascaded H-bridge multilevel converters and the dc–dc converter topology.

**Marco Liserre** (S'00–M'02–SM'07–F'13) received the M.Sc. and Ph.D. degrees in electrical engineering from the Polytechnic University of Bari, Bari, Italy, in 1998 and 2002, respectively.

He was an Associate Professor with the Polytechnic University of Bari. In 2012, he was a Professor of Reliable Power Electronics with Aalborg University, Aalborg, Denmark. Since 2013, he has been a Full Professor and holds the Chair of Power Electronics with the Christian-Albrechts-Universität zu Kiel, Kiel, Germany. He has authored or coauthored 400 technical papers (more than one-third of them in international peer-reviewed journals) and a book. These works have received more than 28 000 citations.

Dr. Liserre was listed in the ISI Thomson report "The world's most influential scientific minds" in 2014. He received an European Research Council Consolidator Grant for the project "The Highly Efficient And Reliable smart Transformer (HEART), a new Heart for the Electric Distribution System." He is a member of the IEEE Industry Applications Society, the IEEE Power Electronics Society (PELS), the IEEE Power and Energy Society, and the IEEE Industrial Electronics Society (IES). He has been serving all these societies in different capacities. He has received the IES 2009 Early Career Award, the IES 2011 Anthony J. Hornfeck Service Award, the 2014 Dr. Bimal Bose Energy Systems Award, the 2011 Industrial Electronics Magazine Best Paper Award, and the Third Prize Paper Award by the Industrial Power Converter Committee at the 2012 IEEE Energy Conversion Congress and Exposition, the 2017 IEEE PELS Sustainable Energy Systems Technical Achievement Award, and the 2018 IEEE IES Mittelmann Achievement Award.